scientific reports

OPEN

Spongy-looking microfabrics in the earliest named stromatolite represent deep burial alteration and incipient metamorphism

Fritz Neuweiler[1✉], Mathias Mueller[2], Benjamin F. Walter[3,4], Ed Landing[5], Aratz Beranoaguirre[3,6], Consuelo Sendino[7,8], Lisa Amati[5] & Stephen Kershaw[8,9]

The earliest named stromatolite *Cryptozoon* Hall, 1884 (Late Cambrian, ca. 490 Ma, eastern New York State), was recently re-interpreted as an interlayered microbial mat and non-spiculate (keratosan) sponge deposit. This "classic stromatolite" is prominent in a fundamental debate concerning the significance or even existence of non-spiculate sponges in carbonate rocks from the Neoproterozoic (Tonian) onwards. *Cryptozoon* has three types of microbially-induced carbonate layers: clotted-pelletoidal micrite with microbial filaments, clotted-pelletoidal micrite with vesicular structure, and dense microcrystalline laminae. A fourth, stratiform to patchy fabric comprises suspect sponges. Using contextual fabric analysis, elemental mapping, cathodoluminescence, fluid inclusions, electron backscatter diffraction, U–Pb dating, and burial history, the sponge interpretation is denied. Neither a distinct sponge body outline nor a canal system is identifiable. Instead, the suspect fabric is secondary in origin, and best explained as a product of Carboniferous (Mississippian) deep burial alteration associated with basement reactivation. Key petrographic observations include heterogenous recrystallization via aggrading Ostwald ripening with interfingering reaction fronts typical for partially miscible fluids, a granoblastic calcite texture (incipient metamorphism), and subsequent hypidioblastic white mica (arguably Carboniferous/Permian, Alleghenian orogeny). Topotype *Cryptozoon* is a stromatolite altered to sub-greenschist metacarbonate. The published Tonian to Phanerozoic record of interpreted non-spiculate sponges requires reassessment.

Keywords Cambrian, Sponges, Appalachian mountains, Fluid inclusions, U–Pb dating, Reactive fluid flow

A current controversy of our understanding of Earth's biotic evolutionary history involves the presence of non-spiculate (spongin-bearing; essentially keratosan) sponges[1] in carbonate rocks from the Neoproterozoic (Tonian) onwards[2–10] (Fig. 1A). With possible exception of a report on an interpreted Triassic keratosan sponge[10], these studies showcase enigmatic, spongy-looking microfabrics characterized by narrow, curved, branching, vesicular to irregular areas of calcite spar embedded in microcrystalline to pelletoidal carbonate. The interpretation of these structures as sponges is based solely on microscopic lookalikes comparing modern keratosan spongin networks with carbonate microcrystalline-spar networks[2,3] (Fig. 2). However, scepticism has arisen[7,9] due to uncertainties regarding fossilization pathways, the reliability of taxonomic conclusions based on a simple microfabric, and in the case of the Tonian material[6], its great age when considering proposed time-resolved molecular sponge phylogeny[11,12]. The accurate identification of non-spiculate sponges in the fossil record holds significant implications for our understanding of early animal evolution, biotic recovery from mass extinctions, and the trophic structure of ancient ecosystems (Fig. 1A).

[1]Département de Géologie et de Génie géologique, Université Laval, 1065, av. de la Médecine, Quebec G1V 0A6, Canada. [2]Institute of Geology, Mineralogy and Geophysics, Ruhr-University Bochum, Universitätsstraße 150, 44801 Bochum, Germany. [3]Karlsruhe Institute for Technology (KIT), Adenauerring 20b, 76131 Karlsruhe, Germany. [4]Department of Geoscience, Petrology and Mineral Ressources, Eberhard Karls University Tübingen, Schnarrenbergstrasse 94-96, 72074 Tübingen, Germany. [5]New York State Museum, 222 Madison Avenue, Albany, NY 12230, USA. [6]Department of Geosciences, Goethe-University Frankfurt, Altenhöferallee 1, 60438 Frankfurt, Germany. [7]Collections Department, National Museum of Natural Sciences, José Gutierrez Abascal 2, Madrid 28006, Spain. [8]Science Group, Natural History Museum, Cromwell Road, London SW7 5BD, UK. [9]Department of Life Sciences, Brunel University London, Uxbridge UB8 3PH, UK. ✉email: Fritz.Neuweiler@ggl.ulaval.ca

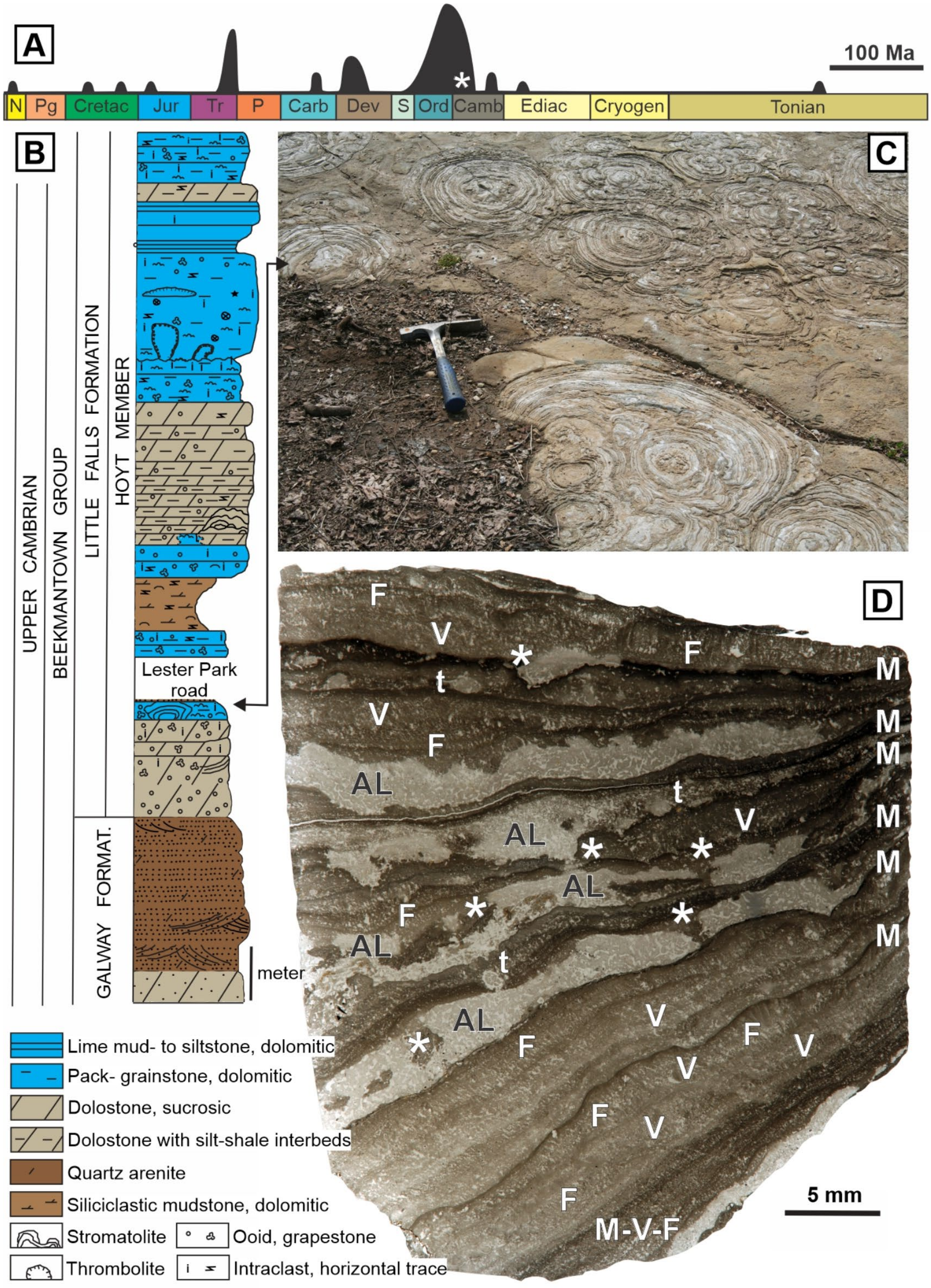

This study re-examines the earliest named stromatolite *Cryptozoon* Hall, 1884 (Fig. 1B–D) that has been interpreted[4] to contain significant (25%) volumes of fossilised non-spiculate sponges. The *Cryptozoon* type horizon is located in Upper Cambrian (ca. 490 Ma) strata immediately east of Lester Park Road in Lester Park, eastern New York State (43° 05′ 28′′ N, 73° 50′ 53′′ W). In this study, "Late" and "Upper" Cambrian refers to a precisely defined proposed subperiod[13], replacing the commonly used but undefined term "late" and "upper" Cambrian of many reports.

Our aim is to reassess the composition and structure of *Cryptozoon* (Fig. 1B–D) to evaluate the sponge hypothesis. This aim is addressed by analysing its fabrics petrographically and geochemically to determine their value in our understanding of the Cambrian evolutionary fauna[14] (Fig. 1A). Thus, we approach alternative explanations of the suspect sponge structure in *Cryptozoon*, necessarily considering diagenesis and burial history by performing a multi-proxy, whole-rock petrogenetic analysis. In a broader perspective, it is expected

◀**Fig. 1**. Introducing Late Cambrian *Cryptozoon* Hall 1884. (**A**) Summary of reports of Neoproterozoic to Phanerozoic carbonate rock microfabrics interpreted as non-spiculate (essentially keratosan) sponges; relative frequency of reports redrawn from[5]. Asterisk indicates the age of our test case, topotype *Cryptozoon* Hall 1884. (**B**) Stratigraphic section (Late Cambrian, Lester Park, Greenfield Township, Saratoga County, New York State, 43° 05′ 28′′ N, 73° 50′ 53′′ W)[15]. *Cryptozoon* formed under marginal-marine conditions correlated with highstand system tracts. Lower part of section contains the morphospecies *C. proliferum*; upper part contains *C. ruedemanni* and *C. undulatum*[59]. (**C**) Disconformity marked by quartz sand layer on beveled surface of *C. proliferum*. (**D**) Scan of thin section of *C. proliferum* (hypotype NYSM 19,458.1) displaying three kinds of primary laminae-layers: densely-clotted pelletoidal micrite with microbial filaments (F), locally tufted; loosely-clotted pelletoidal micrite with vesicular microfabric (V), and dense microcrystalline laminae (M). A fourth, stratiform to patchy fabric (AL) represents suspect sponges[4]. However, these domains cross-cut the primary layering and contain relic structures (asterisks) indicating recrystallisation or neomorphism. Note finger-like protrusions of AL domains. There are peculiar traces (t) of possible biogenic origin (recrystallized, no relic structures).

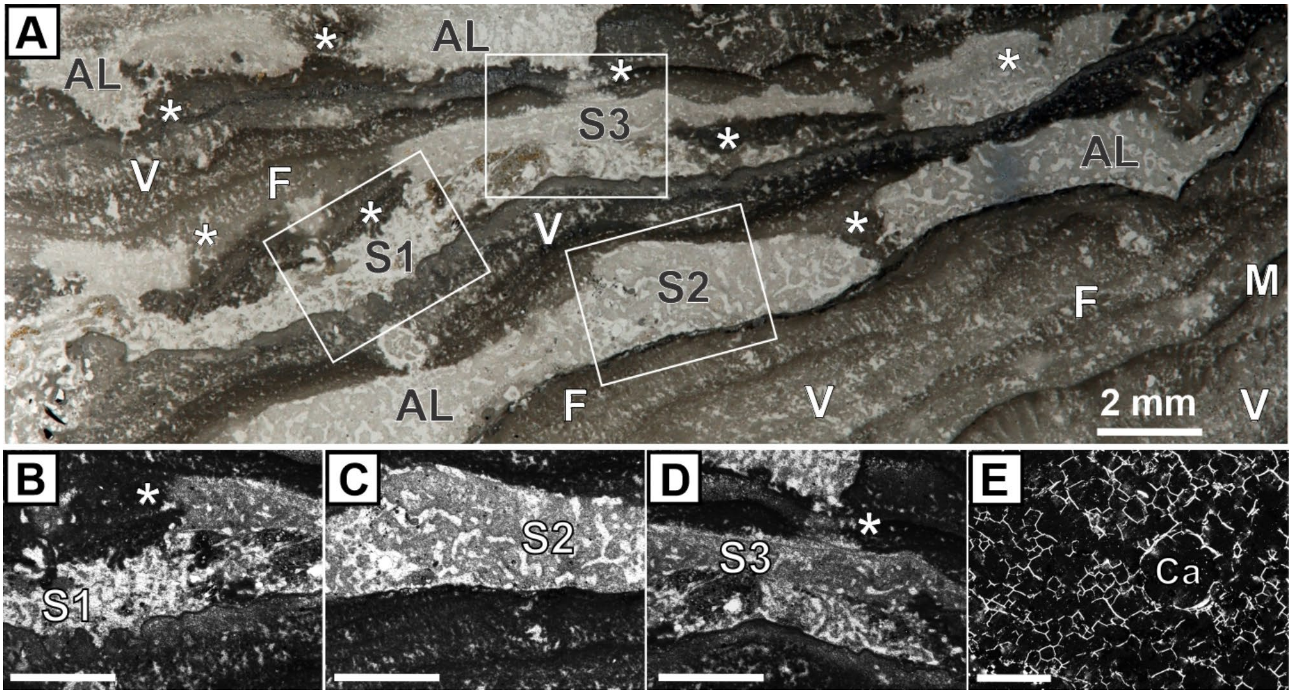

Fig. 2. The secondary nature of spongy microfabrics; close-ups of central part of Fig. 1D. **(A)** Stromatolite layers (F, V, M) and alteration areas (AL) that locally contain relic structures of the host rock (asterisks) and show diffuse, interfingering to scalloped-cuspate margins (asterisks). **(B–D)** Altered areas (AL) show a variety of secondary spongy microfabrics (S1-S3) in function of the nature of the encountered host (granularity, initial spar component). Hypotype NYSM 19,458.1. **(E)** For comparison, cross-polarised light thin-section view of a spongin network of a modern non-spiculate (keratosan) sponge with its distinctive canal system (Ca), spongin is birefringent. For **B–E**, scale bar = 1 mm.

that discrete elements of *Cryptozoon* petrogenesis were produced in concert with the incremental evolution of the Appalachian orogen.

As a starting point, to be precise and as reported[4], topotype *Cryptozoon* has layers and patches interpreted[4] their Figs. 3 and 5) as the biohistorical record of non-spiculate (keratosan) sponges making up around 25% of the stromatolite[4] their Fig. 6). Petrographically, these areas correspond to relatively coarse-crystalline, more translucent domains herein labelled "AL" (Figs. 1D and 2). These domains locally contain "spongy-looking" microfabrics (Fig. 2;[4] their Fig. 5).

Results

Key petrographic features

Cryptozoon displays three kinds of primary microbially-induced layering-lamination (Figs. 1D, 2A and 3A): (1) densely clotted–pelletoidal micrite containing vertical filaments ("F", Fig. 1D), (2) loosely clotted–pelletoidal micrite with vesicular structure ("V", Fig. 1D), and (3) structureless microcrystalline carbonate ("M", Fig. 1D). The transition between F and V fabrics is gradual both vertically and horizontally, while laminae of M fabric remain distinct and continuous at mesoscopic scale (Fig. 1D). Layers dominated by filaments (F) tend to exhibit

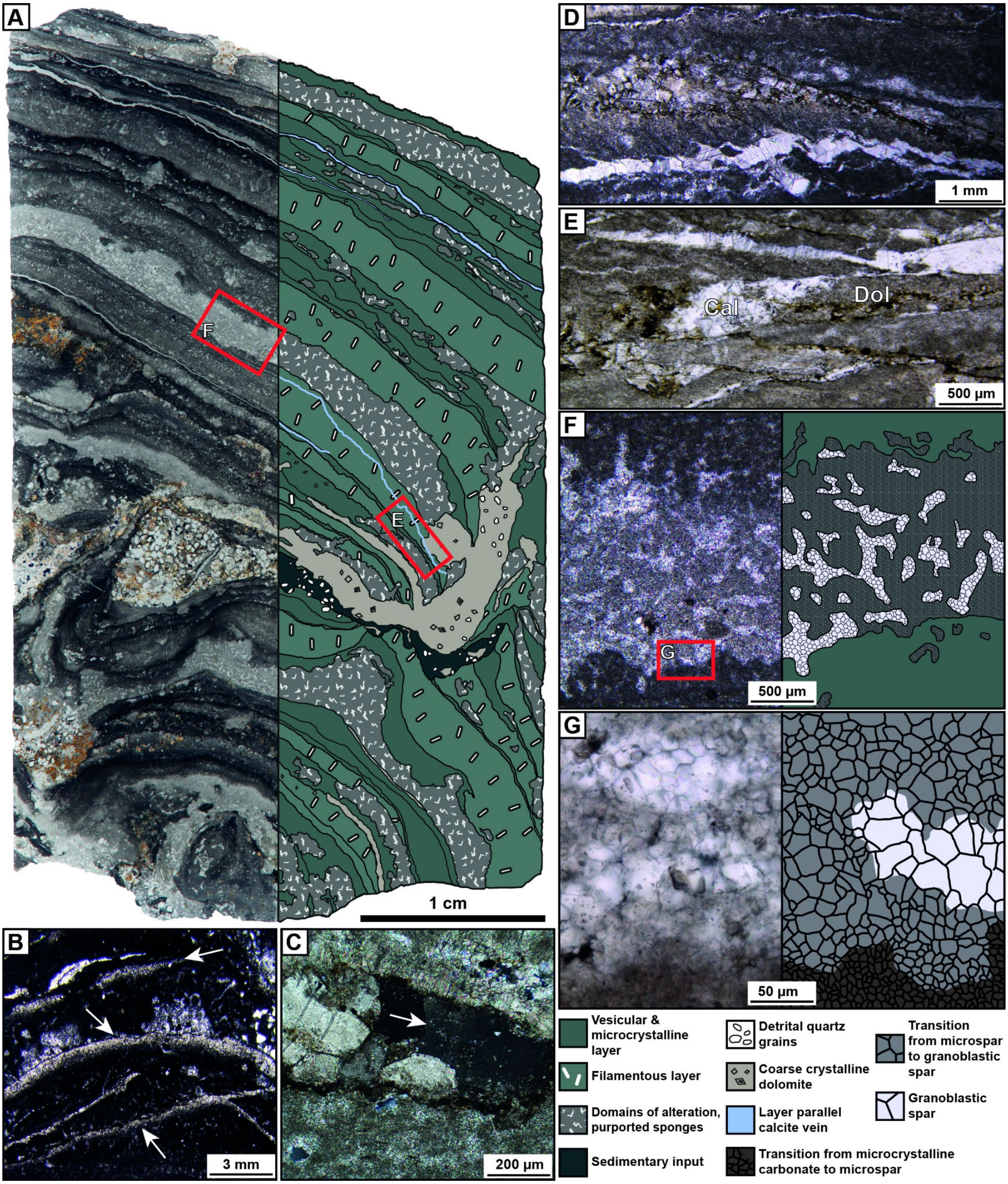

tufted structures, resulting in subtle positive accretionary relief (Fig. 1D). A fourth fabric with a localized spongy appearance is a product of alteration ("AL", Figs. 1D and 2A–D) as it is gradational between the other three, with irregular contacts and relic structures, and critically cuts across the three kinds of primary layering-lamination (asterisks in Figs. 1D and 2). Siliciclastic detritus occurs locally, including silt- to sand-sized quartz, muscovite and chlorite, with minor amounts of feldspar and argillaceous material. The carbonate sedimentary rock surrounding the stromatolite is essentially a packstone with a variety of skeletal bioclasts, stromatolite rip-up clasts, and ooids.

The filamentous and vesicular fabrics contain early centripetal calcite cement after primary fabric-selective porosity. Three kinds of dolomite are associated: (1) matrix microdolomite, (2) coarsely crystalline (zoned) dolomite that occurs as mesoscopic patches grading into swarms of microscopic veins (Fig. 3A, B), and locally, (3) pervasive (zoned) dolomite (see supplementary information file). The coarse-crystalline (zoned) dolomite

◀**Fig. 3**. Lester Park *Cryptozoon*—key petrographic features. (**A**) Mesoscopic context of key petrographic attributes of *C. proliferum*; right-hand half of image shown as a simplified drawing. Note that layer-parallel calcite veins crosscut the primary layers and the coarse-crystalline dolomite but in no case the domains of alteration (purported sponge[4]); from hypotype NYSM 19,458.2. **(B)** Swarm of veins containing (brownish) coarse-crystalline dolomite. **(C)** The coarse-crystalline dolomite displays subtly warped crystal faces and a faint undulose extinction (saddle dolomite). This fabric element contains information (from fluid inclusions, U-Pb dating, Fig. 4F–G) indicating Ordovician hydrothermal alteration. **(D)** Pressure-dissolution associated, layer-parallel calcite veins associated with some coarse-crystalline dolomite, subsequently sheared and micro-faulted. **(E)** Layer-parallel calcite vein cutting across a domain of coarse-crystalline (hydrothermal) dolomite (close-up of **A**). The vein calcite contains information (from fluid inclusions, U-Pb dating, Fig. 4F, I) indicating a Silurian hydrothermal fracture-filling cement. **(F)** Spongy microfabric highlighting the secondary (replacive) nature of semi-translucent domains (close-up of **A**). Right-hand half of image shown as a simplified drawing. **(E)** Details of the spar component of spongy microfabric with its granoblastic center highlighting successive grain boundary area reduction (close-up of **F**; right-hand half of image shown as a simplified drawing).

displays subtly warped crystal faces and subtle undulose extinction (Fig. 3C; saddle dolomite). Following the formation of coarse-crystalline dolomite, pressure-dissolution associated layer-parallel calcite veins formed (Fig. 3A, D, E).

The dolomitization is subtle to pervasive and, even in the latter case, did not obliterate basic early fabric relationships as indicated by manganese-maps (micro-XRF, see supplementary information file). Respective cathodoluminescence reveals dark-bright red luminescent zoned-euhedral and anhedral dolomite (Fig. 4A, B). Vein-related calcite displays a zoned, bright orange-red luminescence, with local resorption of dolomite evident by embayed texture (Fig. 4A, B).

The domains of suspect sponges ("AL" in Figs. 1D and 2) are distinct by their translucence (relatively coarse mean crystal size) and by containing relic structures of the primary layering demonstrating recrystallization (mineral-preserving) or neomorphism. This transformation was heterogenous, it preferentially affected the primary vesicular (V) layers (Figs. 1D and 2A). These domains of alteration display diffuse edges, but locally show distinctly protruding to interfingering, or even sharp boundaries (Figs. 1D, 2 and 3F). Locally, a "spongy-looking" microfabric developed, that is relatively spar-rich areas tending toward spar-interconnection (Fig. 2B–D).

Cathodoluminescence corroborates recrystallization preferring primary vesicular layers, and is shown by patchy bright-red to bright-orange luminescent calcite (Fig. 4C, D). Respective response diminishes diffusively toward the primary filamentous layer (F) and (more distinctly) toward the primary microcrystalline (M) laminae (Fig. 4C, D).

The paragenetic context of the domains of alteration (suspect sponges; "AL" in Figs. 1D and 2A), at first sight, appears somehow perplexing. These domains appear to be replacive and driven by reactive fluid flow (patchy, relic structures, fingering, diffuse boundaries). By the same token, layer-parallel calcite veins crosscut the primary microbial layers and the coarse-crystalline dolomite but in no case the domains of alteration (Fig. 3A, E). Also, the domains of alteration do not crosscut (pass through) layer-parallel calcite veins (Fig. 3A).

The spar component of the secondary "spongy-looking" microfabric contains a centered granoblastic (= polygonal) limpid calcite (Fig. 3F, G) surrounded by interlobate crystal aggregates which grade into a microcrystalline phase (Figs. 3G and 5A). There is one case of a hypidioblastic white mica that precipitated from within an assemblage of coarse dolomite and vein-related calcite (Fig. 4E). There are (at least) two subsequent events: shearing and microfaulting (extensional, dextral; Fig. 3D) and the formation of Fe-calcite cemented microfissures.

Coarse-crystalline dolomite, calcite veins: fluid inclusions, U–Pb dating

Fluid inclusion data were obtained from the relatively early coarse-crystalline (zoned) dolomite and subsequent layer-parallel calcite veins. The measured values (Fig. 4F) provide a T_h range of 119–141 °C for the dolomite, with a salinity of 7.6–9.5 wt% $NaCl_{eq}$, and for the vein-calcite 138–155 °C with 1.1–6.5 wt% $NaCl_{eq}$. U–Pb dating yields a dolomite age of 466 ± 16 Ma and 458 ± 10 Ma (Fig. 4G, H). This roughly brackets the Middle–Late Ordovician boundary interval, coincident with the Taconian orogeny[15–17], and ranges through most of the Late Ordovician. The vein-calcite formed at around 432 ± 9 Ma (Fig. 4I) and brackets most of the lower to mid Silurian (lower Llandovery, Wenlock). The Silurian age bracket is coincident with the Salinic orogeny[16–18], as commonly reported from the more northern Appalachian regions[19–21].

Spongy-looking fabrics: crystallographic preferred orientation, U–Pb dating

EBSD analysis explored crystallographic preferred orientation (CPO, Fig. 5A–C) covering two neighboring domains, from fine-crystalline carbonate (microspar) into interlobate-granoblastic spar. This analysis shows a haphazard orientation in pole figures irrespective of the methodological bias caused by the few largest grains (Fig. 5B, C, see supplementary information file). U–Pb dating (Fig. 5D, E) provides an age of 356 ± 8 Ma for the relatively fine-crystalline carbonate, and 341 ± 7 Ma for the spar component. A 356 ± 8 Ma age brackets the Late Devonian (Famennian) through early Carboniferous (Mississippian, Tournaisian) and overlaps the later stages of the Neo-Acadian[22] orogeny[16] for review and discussion). The significantly younger (341 ± 7 Ma) spar component is coeval with regional dextral shear, basement reactivation and sedimentary basin formation in the northern Appalachians[16,17,23]. This time corridor is prior to deepest regional burial (late Carboniferous, early

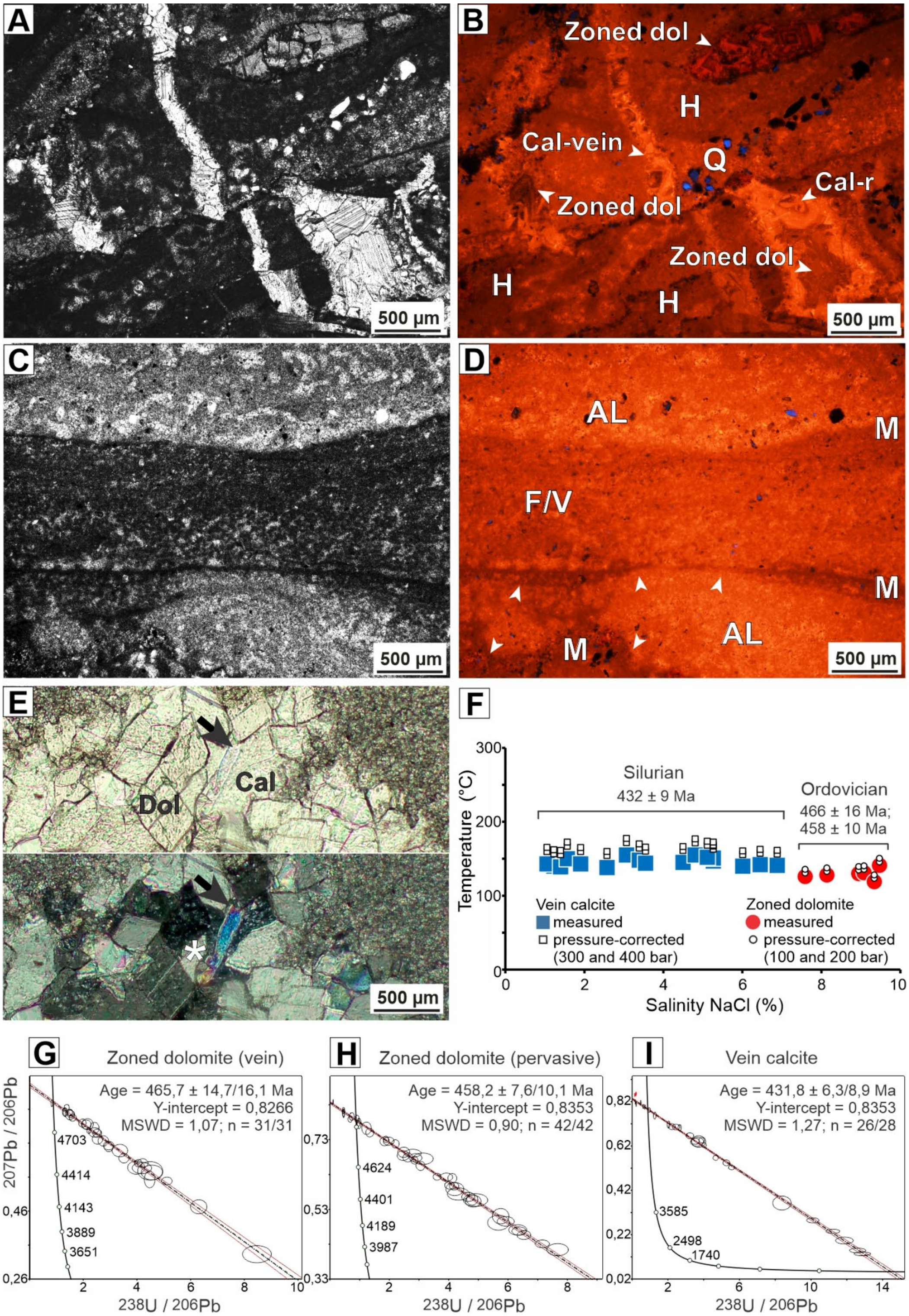

Permian) accounting for anthracite-grade burial in the Appalachians of eastern Pennsylvania[24,25]. Interestingly, these neighboring petrographic domains contain U–Pb data outliers plotting with opposite offset (Fig. 5D, E).

Discussion
Regional burial history
The geological history of the Adirondack domal uplift and the broader eastern New York region (including Lester Park) shows evidence of interim deep burial reaching into incipient (anchizone) metamorphism commonly envisaged at ≥ 200 °C[26,27]. An assessment of the burial history starts from study of anthracite-bearing, Devonian rocks of the Catskill Mountains to the southwest with about 6.5 km of burial[28]. Considering that Late Cambrian *Cryptozoon* strata lie about 1 km below the Catskill Mountain highlands, the total burial depth should have reached 7–8 km (~ 3 kbar, ~ 200 °C). In addition, there is evidence of short-term episodes of elevated crustal heat

◂**Fig. 4**. Lester Park *Cryptozoon*–cathodoluminescence; authigenic mica, fluid inclusions, U–Pb dating. (**A**, **B**) Paired micrographs displaying the *Cryptozoon* host rock (H) affected by hydrothermal dolomite (zoned-dol), by itself dissected or partially replaced (embayed texture) by zoned hydrothermal calcite (cal-vein; cal-r[esorption]). From hypotype thin-section NYSM 6508.1. **(C**, **D)** Paired micrographs displaying primary layering comprising vesicular (V), filamentous (F) and dense microcrystalline (M) microfabrics. Note diffusive protrusion of bright orange cathodoluminescent area (alteration, AL) into microcrystalline layers (arrows). Note preferential alteration (AL) of the vesicular (top) layer with abundant bright-orange luminescent calcite. From hypotype thin-section NYSM 6508.1. **(E)** PPL (top) and XPL (bottom) showing hypidioblastic white mica subsequent to coarse dolomite (Dol) and dolomite-resorbing vein-calcite (Cal). There are subtle signs of brittle deformation (asterisk). Original NYSM 6511.1 assigned to *C. ruedemanni* from the upper part of the stratigraphic section. **(F)** Fluid inclusion salinity *versus* uncorrected and corrected (estimate) homogenization temperature-plot of zoned dolomite and subsequent zoned calcite (from hypotype NYSM 6508.2). **(G–I)** Tera-Wasserburg isochron plots; uncertainty ellipses represent 2σ. MSWD = mean square of weighted deviates. **(G)** From coarse-crystalline (zoned) dolomite in veins, new thin-section NYSM 6508.2. **(F)** From pervasive coarse-crystalline dolomite, new thin-section NYSM 6517.2. **(G)** From subsequent vein-calcite, NYSM 6508.2.

flow during burial, as suggested by a petroleum geology-based study[29]. The maximum burial depth was reached during the late Paleozoic (late Carboniferous; early Permian) Alleghenian orogeny[24,25]. Studies on uplift[30] draw a connection with the Neotethyan-Atlantic regime and Mesozoic heating associated with the Great Meteor (or New England) Hotspot Track. From Jurassic to Cretaceous, the unroofing of the Adirondack domal uplift was accompanied by intrusion of mafic dikes[31].

In the larger context of the Appalachian orogen, the thermal maturity of the area of study roughly follows major structural trends[32,33]. The Ordovician of the Saratoga county (including Lester Park) is in continuation with a regional Conodont Alteration Index (CAI) isograd of 4.5[33]. Such a CAI (time, temperature) translates into maximum burial temperatures well above 200 °C.

Time-resolved petrogenesis

This study corroborates prior findings[25] that during the late Middle to Late Ordovician (= Taconian orogeny), Late Cambrian *Cryptozoon* strata underwent hydrothermal alteration that introduced coarse-crystalline, zoned (saddle) dolomite, whether recorded as swarms of microscopic veins, as mesoscopic patch or even pervasive dolomite (Figs. 3A–E, 4A and B and 6; supplementary information file;[34]for review on saddle dolomite;[35]for review on hydrofractures in rocks). Hydrothermal alteration occurred while the Cambrian strata were still in a shallow-burial environment, affected by medium salinity (7.6 to 9.5 wt% NaCl) fluids at 123–151 °C applying an estimated pressure range of 100–200 bar (Fig. 4F; supplementary information file).

Layer-parallel calcite veins formed during the lower to mid Silurian stage of burial of Late Cambrian strata, and are probably related to mechanical fracturing associated with pressure dissolution and a specific episode of rapid fluid expulsion[29]. Respective fluid inclusions indicate low salinity fluids though with a large range (1.1–6.5 wt% NaCl) at 154–177 °C applying an estimated pressure range of 300–400 bar (Fig. 4F; supplementary information file). Taken together, calcite vein formation must be considered in conjunction with another pulse of crustal heat flow (Fig. 6; Salinic hydrothermal calcite). The large range of salinity of vein calcite-hosted fluid inclusions might imply, at first sight, a non-cogenetic origin. However, fluid inclusions that show any kind of evidence of post-entrapment modification were not analyzed (see "Methodology" section). It is worth noting that primary fluid inclusions on a single growth zone may vary significantly in major and trace elements as well as in salinity and T_h in function of various states of fluid mixing (here eventually a dilute meteoric fluid and a brine) together with the effects of crystal growth kinetics[36–38].

The paragenetic status of the domains of alteration-recrystallisation ("AL" fabric, suspect sponges[4]; Figs. 1D, 2A and 3A), though puzzling by conventional optical petrography, by U–Pb dating turns out to be late Paleozoic (essentially Carboniferous) in age, thus indicating a deep burial origin (Figs. 5D and E and 6). According to the regional burial history, this time corridor includes conditions where deep burial diagenesis of Late Cambrian strata might have reached into the realm of incipient metamorphism[24,25]. Our data indicate that this transition started to come into play during the Mississippian period (Fig. 5D, E).

Certain consequences arise: The domains of alteration (suspect sponges[4]) are a distinct play by petrography, burial status and age, rather geothermal than hydrothermal in origin and clearly postdating both the hydrothermal dolomite and the hydrothermal calcite (Figs. 3A–E, 4G and H, 5D and E and 6). In our understanding, newly introduced fluids encountered a highly heterogeneous poro-perm carbonate medium with primary (Late Cambrian) microcrystalline layers and (Silurian) layer-parallel calcite veins acting as fluid barriers (ambiguity of optical petrography in Fig. 3A is thus resolved). Primary vesicular layers were preferentially altered (Figs. 1D, 2, 3A and 4C and D) likewise due to their effective intercrystalline permeability (vesicular spar component, fingering) enclosing microcrystalline carbonate (high surface area). This scenario matches well the process and products of self-focused reactive fluid flow[39–41] promoting aggrading recrystallisation (Ostwald ripening). Eventually, the distant effects of tectonic expulsion of formation fluids toward foreland areas might apply, that is a Mississippian "hot flash" kind of squeegee-type fluid flow regime[24,42–46].

Aggrading recrystallisation (Carboniferous, Fig. 6) did not produce a distinct CPO (Fig. 5A–C), in contrast to, e.g., high pressure marble[47]. Thus, static recrystallisation prevailed *via* grain-into-grain boundary migration (interlobate calcite) and successive grain boundary area reduction tending toward polygonal calcite (Figs. 3G and 6)[48]. Thus, fluid-driven alteration passed into more diffusion-controlled solid-state reorganization[49].

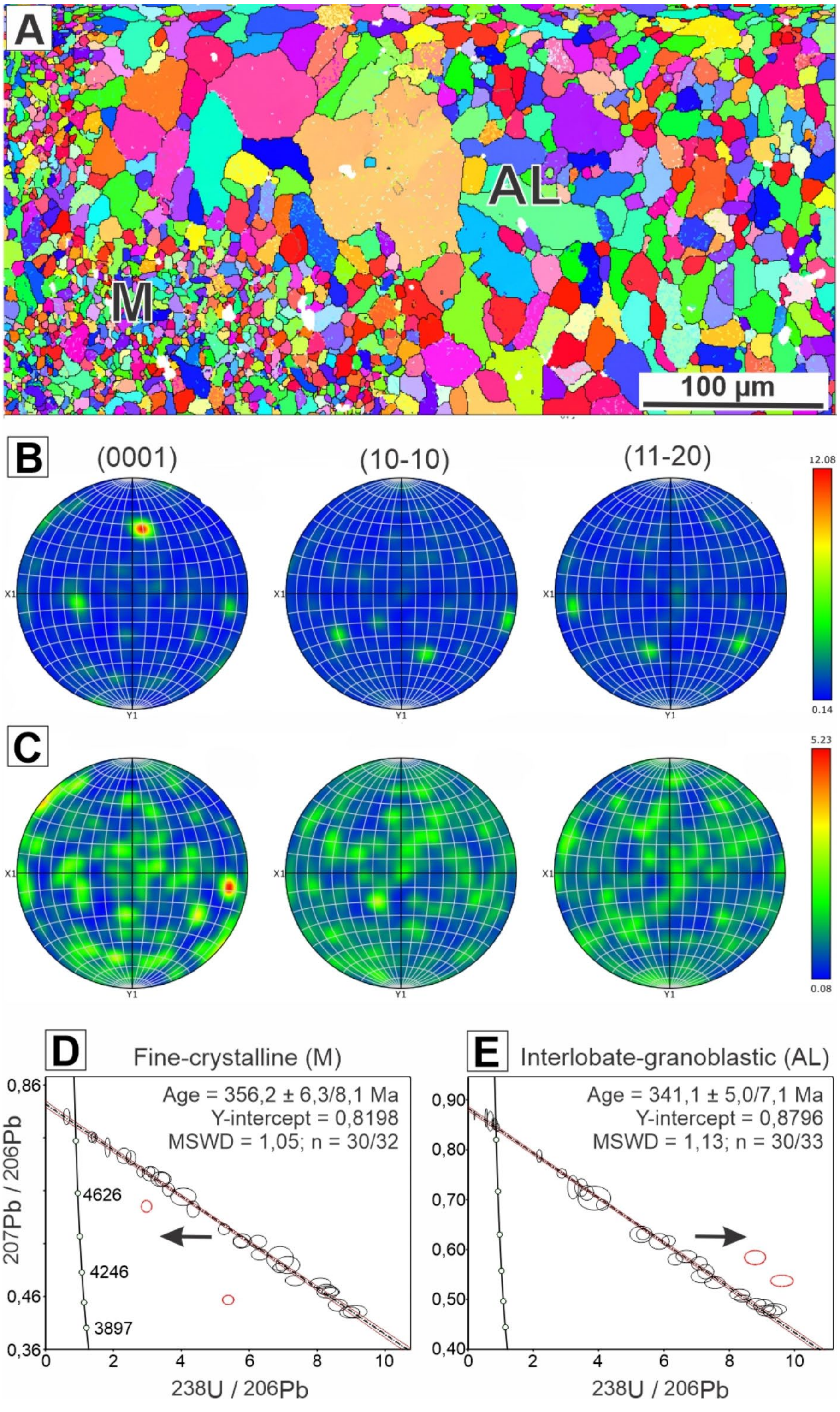

Fig. 5. Crystallographic orientation data of a spongy-looking microfabric, U–Pb dating. **(A)** Crystallographic orientation analysis of two neighboring domains, from fine-crystalline carbonate (M) into interlobate-granoblastic spar (AL). White spots indicate non-calcite mineralogy. **(B)** Indistinct preferred orientation in pole figures of the entire area with strong bias induced by the few largest grains. **(C)** Haphazard orientation in pole figures of the entire area after excluding the few largest grains. From hypotype thin-section NYSM 6508.1. **(D, E)** Tera-Wasserburg isochron plots; uncertainty ellipses represent 2σ; MSWD = mean square of weighted deviates; arrows indicate potential open system behavior[52]. **(D)** From fine-crystalline domain; **(E)** from spar-rich (interlobate-granoblastic) domain (hypotype NYSM 6508.1).

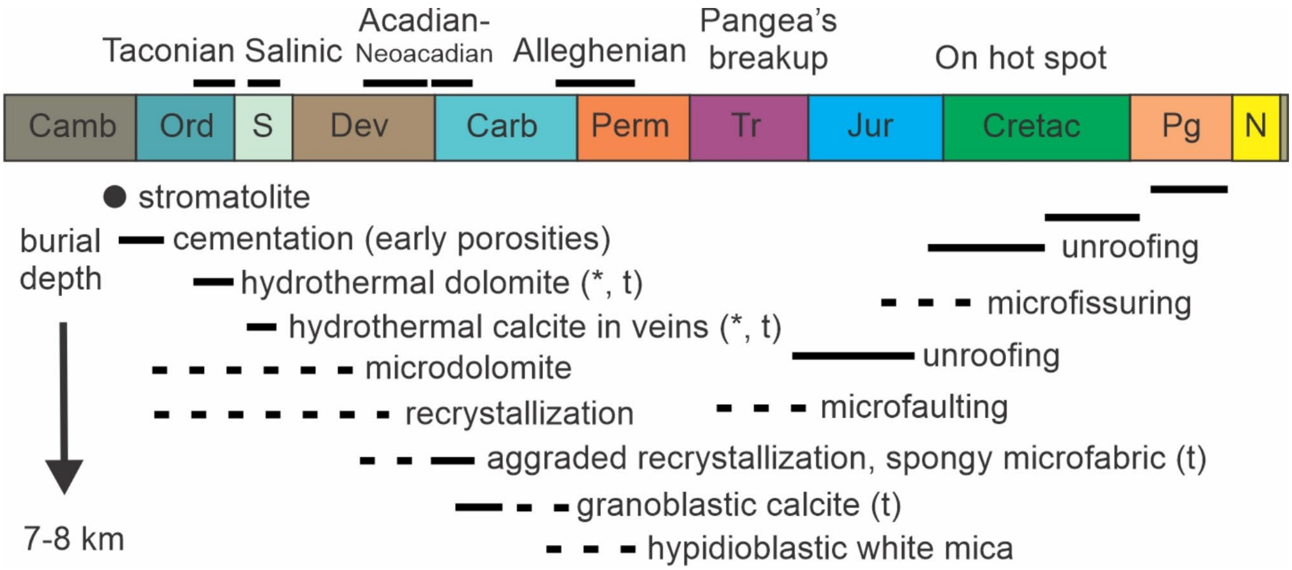

Fig. 6. Time-resolved petrogenesis of topotype *Cryptozoon*. Key petrographic features (simplified, burial depth not to scale) in the context of the regional structural evolution. Asterisk refers to interconnected fluid inclusion data (Fig. 4F), t refers to interconnected U–Pb dating (Figs. 4G–I and 5D and E).

Whereas the polygonal granoblastic calcite subtly indicates incipient metamorphism of a highly reactive carbonate medium, the hypidioblastic white mica (Fig. 4E) is considered to be subsequent and low-metamorphic in nature with feldspar acting as a reactor (Fig. 6). However, caution is required, as this white mica is a first, and so far discovered, single finding. It occurs in the upper part of the stratigraphic section (Figs. 1B and 4E). This interpretation makes sense because the potential source of relative abundant feldspar in the Lester Park area is the gneissic basement of the Mesoproterozoic Grenville Orogen. However, the Grenville is "sealed" as a feldspar source by non-conformably overlying Cambrian units that essentially lack feldspar[50]. There is a coarse-grained, dolomitic sandstone with abundant feldspar that follows truncation of Lester Park buildups[50] likely derived by erosion of older units with sea-level fall. Here, more examples are needed to eventually determine the respective muscovite-phengite ratio[51] and the geochronological signature. Overall, the earliest named stromatolite *Cryptozoon* Hall, 1884 displays petrographic evidence of low-grade (sub-greenschist) metamorphism in good accord with regional thermal maturity patterns obtained from Ordovician Conodont Alteration isograds[33].

Exploring the U–Pb age difference (~ 10 Ma) together with outliers recorded in fine-crystalline *versus* spar domains of spongy-looking microfabrics (Fig. 5D, E), again, requires an enlarged dataset. Possible explanations include uranium and/or lead mobility (open(d) system behavior) during deep burial alteration[52]. No Mesozoic mafic dike is reported from the area of study, and post-Paleozoic thermal/hydrothermal alteration seems unlikely.

In summary (Fig. 6), a late Paleozoic (Mississippian) transition from deep burial diagenesis into incipient sub-greenschist metamorphism is concluded for the succession of domains of alteration/recrystallisation ("AL" in Fig. 1D; suspect sponges[4]), locally developing a spongy microfabric (Fig. 2), with subsequent granoblastic calcite (Fig. 3G) and hypidioblastic white mica (Fig. 4E). Extensional micro-faulting (Fig. 3D), the subtle brittle deformation of white mica (Fig. 4E), and Fe-calcite cemented fissures are subsequent, arguably related to Pangea's breakup[53], uplift and Mesozoic unroofing (Fig. 6).

No evidence for keratosan sponges in Late Cambrian *Cryptozoon* Hall, 1884

Two kinds of key observation call the presence of keratosan sponges in *Cryptozoon* into question. First, considering the domains of alteration/recrystallization (suspect sponges, 25% of rock volume[4]) and by carefully observing associated relic (ghost) structures (Figs. 1D and 2), the primary tripartite architecture and layering of the stromatolite laterally is sustained. Importantly, the vesicular and filamentous layers grade into each other (Figs. 1D and 2), vertically and horizontally. However, distinct (metazoan) organisms do not grade into each other, but (microbial) communities and resulting rock fabrics may. Going back to the late 1970s and early 1980s, such vesicular (or micro-fenestrate) and filamentous layers of microbial mats/stromatolites have been conceptualized as spongiostromate and porostromate microbial (cryptalgal) fabrics, whereby lateral and vertical changes in microstructure are related to changes in the building (microbial) communities and/or in their environmental interactions[54,55]. Second, there are no spongy-looking microfabrics outside the domains of alteration. The domains of alteration contain no relics indicating a distinct sponge-body outline, and there is no evidence for the sponge-defining[56] canal system (Fig. 2E).

Because there is not one single item of positive evidence, the suspect non-spiculate sponge fossils[4] in topotype *Cryptozoon* are considered a pseudofossil. Respective domains (Figs. 1D, 2A–D, 3A and F–G, 4C, D and 5A–C) are best explained by reorganization of carbonate rock fabric due to (tectonically-induced?) fluid injection within the deep burial realm. Intercrystalline effective permeability, self-focused reactive fluid flow, fluid miscibility, reaction front (viscous) fingering and grain boundary migration (-area reduction) are considered critical elements of such alteration. We conclude that topotype *Cryptozoon* is a stromatolite altered to sub-greenschist metacarbonate devoid of non-spiculate sponges. Our case highlights the extra caution needed when interpreting fabrics of carbonate stromatolites (or fine-grained carbonate rocks in general) which have undergone heterogenous recrystallisation.

Spongy-looking microfabrics in carbonate rocks have very different origins, comprising recrystallization-neomorphism, fluid flow/capture, burrowing, nesting, and tunneling meiofauna[7,9]. This contribution demonstrates the importance of multi-proxy, contextual fabric analysis in the evaluation of biotic-taxonomic interpretation and that future studies should follow this approach. The effects of aggraded recrystallisation (neomorphism) are notorious in our understanding of a number of Precambrian and Cambrian carbonate stromatolites[57]. Our *Cryptozoon* case might shed some light on why "fossil (keratosan) sponges" frequently have been reported from thin-sections of deeply buried early Paleozoic fine-grained carbonate rocks (Fig. 1A). As a starting point, a critical re-examination of associated key studies[5,58] is suggested (exhaustive list in[9], their supplement file). The proposed genetic rock term "keratolite"[5] should be re-evaluated.

Finally, the much younger, earliest Triassic acme of reported non-spiculate (keratosan) sponges (Fig. 1A) is a very separate case as suspect structures are fundamentally different by context, petrography and burial history[7,9]. In any case, we encourage careful consideration of the full range of biotic-taxonomic and abiotic-diagenetic options, applying an open-minded, multi-proxy contextual fabric analysis before concluding for a far-reaching re-assessment[5] of our understanding of sponge (animal) evolution (Fig. 1A).

Methodology

Our study used topotype *Cryptozoon* material[59] from the New York State Museum (NYSM) that was collected from the prominent exposure surface immediately east of Lester Park Road (Fig. 1B, C). In addition, new thin-sections were prepared from Goldring's[59] slabs and examined under plane-polarized light (PPL), cross-polarized light (XPL) and optical microscopy-cathodoluminescence (OM-CL). Lester Park is a protected natural geoheritage site of the NYSM[18]. The material is reposited under NYSM hypotype numbers.

Optical microscopy, element mapping, crystallographic orientation

Polarized images were taken on a Leica DM4500P microscope (Leica Microsystems GmbH, Wetzlar, Germany). Cathodoluminescence analyses were performed using a hot cathode (HC1-LM) facility at the Ruhr-University Bochum[60] equipped with a DC73 camera system (Olympus). Thin sections were sputter coated with a 15 nm-thick gold layer to avoid charging. The electron beam had an acceleration voltage of 14 kV, a current density of 5–10 µA/mm², and a beam current of 0.1–0.2 mA. Dolomite and calcite cement phases were identified based on optical relief, luminescence colors[61] and textural criteria. Major and minor element chemical maps were produced using a micro-XRF device (Bruker M4 TORNADO at Université Laval). Crystallographic orientation data (EBSD) were collected on a thin section polished with OPS and tilted by 70° using a Symmetry2 electron backscatter detector from OXFORD INSTRUMENTS and a step width of 0.8 µm. The electron beam was set to 20 kV acceleration voltage and 500 pA probe current. EBSD data were collected with AZtec version 6.1. Post-processing of crystal orientation data (removing wild spikes, producing pole figures) was done using AZtecCrystal (https://nano.oxinst.com/azteccrystal).

Fluid inclusions

Microthermometric investigations were performed using a Linkam THMS600 stage at the Karlsruhe Institute of Technology (KIT)[62]. The chronological sequence of fluid inclusion assemblages (FIA[63]) were determined by optical microscopy, with fluid inclusions classified as primary (p), pseudo-secondary (ps), and secondary (s). The only data used for interpretation were triple measurements with reproducible final melting (deviation < 0.1 °C) temperature of ice (Tm ice) and hydrohalite (Tm hh) and the homogenization temperature (T_h). Synthetic H_2O, H_2O-NaCl and H_2O-CO_2 fluid inclusion standards (SynFlinc standards) were used for temperature calibration of the stage. Salinity was calculated by the NaCl-$CaCl_2$-H_2O system[64]. The volume fractions are described by the volume fraction notation based on their phase assemblage at room temperature[65].

U–Pb dating

Uranium-lead age data of carbonate were collected on a ThermoFisher Element XR sector field ICPMS coupled to a 193-nm ArF excimer laser with a HelEx 2-volume cell (Analyte Excite+, Teledyne Photon Machines) at the Laboratory for Environmental and Raw Materials Analysis (LERA), Karlsruhe Institute for Technology (Germany), and were slightly modified from[66]. The data were acquired in one analytical session in November 2023; see supplementary information file for analytical parameters (spot size, repetition rate, acquisition times, gas flows). The $^{207}Pb/^{206}Pb$ and $^{206}Pb/^{238}U$ ratios were corrected for mass bias, including drift over time, using the primary reference material SRMNIST612 glass[67]. An additional correction was applied to the $^{206}Pb/^{238}U$ ratios to account for matrix differences between the primary reference material and carbonate. The correction value was estimated on the common Pb-corrected WC-1[68] and applied to all carbonate samples assuming similar behaviour. Secondary reference calcite materials, B-6[69] and Duff Brown Tan[70] were measured for quality control. Data processing was carried out using an in-house VBA Microsoft Excel spreadsheet program[71]. Uncertainties reflect the quadratic addition of internal uncertainties, counting statistics, background, and the excess of scatter and variance[72].

Data availability

Data is provided within the manuscript and the supplementary information file.

Received: 14 August 2024; Accepted: 13 December 2024
Published online: 28 December 2024

References

1. Erpenbeck, D. et al. Horny sponges and their affairs: on the phylogenetic relationships of keratose sponges. *Mol. Phylogenet. Evol.* **63**, 809–816 (2012).
2. Luo, C. & Reitner, J. First report of fossil keratose demosponges in Phanerozoic carbonates: preservation and 3-D reconstruction. *Naturwissenschaften* **101**, 467–477 (2014).
3. Luo, C. & Reitner, J. Stromatolites' built by sponges and microbes–a new type of Phanerozoic bioconstruction. *Lethaia* **49**, 555–570 (2016).
4. Lee, J. H. & Riding, R. The 'classic stromatolite' *Cryptozoon* is a keratose sponge-microbial consortium. *Geobiology* **19**, 189–198 (2021).
5. Lee, J. H. & Riding, R. Keratolite–stromatolite consortia mimic domical and branched columnar stromatolites. *Palaeogeogr. Palaeoclimatol .Palaeoecol.* **571**, 110288 (2021).
6. Turner, E. C. Possible poriferan body fossils in early Neoproterozoic microbial reefs. *Nature* **596**, 87–91 (2021).
7. Kershaw, S., Li, Q. & Li, Y. Addressing a Phanerozoic carbonate facies conundrum—sponges or clotted micrite? Evidence from early Silurian reefs, South China block. *Sediment. Record* **19**, 3–10 (2021).
8. Luo, C., Pei, Y., Richoz, S., Li, Q. & Reitner, J. Identification and current palaeobiological understanding of Keratosa-type nonspicular demosponge fossils in carbonates: with a new example from the lowermost Triassic. *Armen. Life* **12**, 1348 (2022).
9. Neuweiler, F. et al. Keratose sponges in ancient carbonates—a problem of interpretation. *Sedimentology* **70**, 927–968 (2023).
10. Wu, S., Reitner, J., Harper, D. A. T., Yu, J. & Chen, Z. Q. New keratose sponges after the end-Permian extinction provide insights into biotic recoveries. *Geobiology* **22**, e12582 (2024).
11. Schuster, A. et al. Divergence times in demosponges (Porifera): first insights from new mitogenomes and the inclusion of fossils in a birth-death clock model. *BMC Evol. Biol.* **18**, 114 (2018).
12. Kenny, N. J. et al. Tracing animal genomic evolution with the chromosomal-level assembly of the freshwater sponge *Ephydatia muelleri*. *Nat. Commun.* **11**, 3676 (2020).
13. Landing, E., Geyer, G., Schmitz, M. D., Wotte, T. & Kouchinsky, A. Re)proposal of three Cambrian subsystems and their geochronology. *Episodes* **44**, 273–283 (2021).
14. Carrera, M. C. & Botting, J. P. Evolutionary history of Cambrian spiculate sponges: implications for the Cambrian evolutionary fauna. *Palaios* **23**, 124–138 (2008).
15. Landing, E. (ed) Ediacaran–Ordovician of east Laurentia: S.W. Ford memorial volume, 12th International Conference of the Cambrian Chronostratigraphy Working Group. *Bull. N. Y. State Mus* **510**, 94 (2007).
16. van Staal, C. R. et al. Pre-Carboniferous, episodic accretion-related, orogenesis along the Laurentian margin of the northern Appalachians. In *Ancient Orogens and Modern Analogues* (eds. Murphy, J. B. et al.). *Geol. Soc. Lond. Spec. Publ., vol. 327* 271–316 (2009).
17. Ettensohn, F. R., Pashin, J. C. & Gilliam, W. The Appalachian and Black Warrior Basins: Foreland basins in the eastern United States. In *The Sedimentary Basins of the United States and Canada* (ed. Miall, A.D.) 129–237 (Elsevier, 2019).
18. Landing, E. & Bartholomew, A. J. Lester Park: global type locality for stromatolite fossils. *GSA Today* **34**, 8–12 (2024).
19. van Staal, C. R. et al. Tectonic evolution of high-grade metamorphic tectonites of the Meelpaeg structure near Port aux Basques, southwestern Newfoundland during the Silurian Salinic and Early-to-Middle Devonian Acadian orogenies. *Can. J. Earth Sci. e-First*. https://doi.org/10.1139/cjes-2023-0141
20. Bourque, P. A., Malo, M. & Kirkwood, D. Paleogeography and tectono-sedimentary history at the margin of Laurentia during Silurian to earliest Devonian time: the Gaspé Belt, Québec. *Geol. Soc. Am. Bull.* **112**, 4–20 (2000).
21. Perrot, M. & Tremblay, A. Structural characterization of late Silurian normal faults in the Quebec Appalachians: Implications for sedimentary basin formation and Laurentian margin exhumation during the Salinic orogeny. *J. Struct. Geol.* **150**, 104397 (2021).
22. Robinson, P., Tucker, R. D., Bradley, D., Berry, H. N. & Osberg, P. H. Paleozoic orogens in New England. *USA GFF* **120**, 119–148 (1998).
23. Piette-Lauzière, N., Larson, K. P., Kellett, D. A., Rogers, N. & Powell, J. Late Devonian shear zone reactivation in the Canadian Appalachian orogen. In *Supercontinents, orogenesis and magmatism* (eds. Nance, R. D. et al.) *Geol. Soc. London, Spec. Publ., vol. 542* 287–314 (2023).
24. Levine, J. R. Deep burial of coal-bearing strata, anthracite region, Pennsylvania: sedimentation or tectonics. *Geology* **14**, 577–580 (1986).
25. Heizler, M. T. & Harrison, T. M. The thermal history of the New York basement determined from $^{40}Ar/^{39}Ar$ K-feldspar studies. *J. Geophys. Res.* **103**, 29795–29814 (1998).
26. Immenhauser, A. On the delimitation of the carbonate burial realm. *Deposit. Record* **8**, 524–574 (2022).
27. Bucher, K. Controlling factors of mtamorphism. In *Encyclopedia of Geology* (eds. Alderton, D. & Elias, S. A.) 366–374 (Academic, 2021).
28. Friedman, G. M. & Sanders, J. E. Time-temperature-burial significance of Devonian anthracite implies former great (~6.5 km) depth of burial of Catskill Mountains, New York. *Geology* **10**, 93–96 (1982).
29. O'Reilly, C. & Parnell, J. Fluid flow and thermal histories for Cambrian–Ordovician platform deposits, New York: Evidence from fluid inclusion studies. *Geol. Soc. Am. Bull.* **111**, 1884–1896 (1999).
30. Yang, X. & Gao, H. Full-wave seismic tomography in the northeastern United States: new insights into the uplift mechanism of the Adirondack Mountains. *Geophys. Res. Lett.* **45**, 5992–6000 (2018).
31. Roden-Tice, M. K. & Tice, S. J. Regional-scale Mid-Jurassic to Late Cretaceous un-roofing from the Adirondack Mountains through central New England based on apatite fission-track and (U-Th)/He thermochronology. *J. Geol.* **113**, 535–552 (2015).
32. Harris, A. G., Harris, L. D. & Epstein, J. B. Oil and gas data from Paleozoic rocks in the Appalachian basin: maps for assessing hydrocarbon potential and thermal maturity (conodont color alteration isograds and overburden isopachs). In *U.S. Geological Survey Miscellaneous Investigations*, Map I-917-E, scale 1:2,500,000, 4 sheets (1978).
33. Weary, D. J., Ryder, R. T. & Nyahay, R. Thermal maturity patterns (CAI and %Ro) in the Ordovician and Devonian of the Appalachian Basin in New York State. In *U. S. Geological Survey Open-File Report 00-496* 39 (2000).
34. Zhang, Y. F. et al. Towards an improved understanding of Ca–Mg carbonates with nonplanar surfaces: an experimental approach. *Sedimentology* https://doi.org/10.1111/sed.13228 (2024).
35. Bons, P. D. et al. A review of natural hydrofractures in rocks. *Geol. Mag.* **159**, 1952–1977. https://doi.org/10.1017/S001675682200104 (2023).
36. Walter, B. F. et al. Multi-reservoir fluid mixing processes in rift-related hydrothermal veins, Schwarzwald, SW-Germany. *J. Geochem. Explor.* **186**, 158–186 (2018).
37. Walter, B. F. et al. Chemical evolution of ore-forming brines—basement leaching, metal provenance, and the redox link between barren and ore-bearing hydrothermal veins. A case study from the Schwarzwald mining district in SW-Germany. *Chem. Geol.* **506**, 126–148 (2019).
38. Mueller, M. et al. A tale of three fluids: fluid-inclusion and carbonate clumped-isotope paleothermometry reveals complex dolomitization and dedolomitization history of the Latemar platform. *J. Sed Res.* **92**, 1141–1168 (2022).

39. Chen, W. & Ortoleva, P. Reaction front fingering in carbonate-cemented sandstones. *Earth Sci. Rev.* **29**, 183–198 (1990).
40. Chen, W., Ghaith, A., Park, A. & Ortoleva, P. Diagenesis through coupled processes: modeling approach, self-organization, and implications for exploration. In *Prediction of Reservoir Quality Through Chemical Modeling* (eds. Meshri, I.D & Ortoleva, P.) *Am. Ass. Petrol. Geol. Mem., vol. 49* 103–130 (1990).
41. Morse, J. W. & Casey, W. H. Ostwald processes and mineral paragenesis in sediments. *Am. J. Sci.* **288**, 537–560 (1988).
42. Oliver, J. Fluids expelled tectonically from orogenic belts: their role in hydrocarbon migration and other geologic phenomena. *Geology* **14**, 99–102 (1986).
43. Machel, H. G. & Cavell, P. A. Low-flux, tectonically-induced squeegee fluid flow (hot flash) into the Rocky Mountain Foreland Basin. *Bull. Can. Petrol. Geol.* **47**, 510–533 (1999).
44. Beaudoin, N., Lacombe, O., Hoareau, G. & Callot, J-P. How the geochemistry of syn-kinematic calcite cement depicts past fluid flow and assists structural interpretations: a review of concepts and applications in orogenic forelands. *Geol. Mag.* **159**, 2157–2190 (2023).
45. Evans, M. A. Syntectonic sediment loading and fold-thrust belt structural architecture: An example from the central Appalachians (USA). *Geosphere*, 19: 449–470 (2023).
46. Evans, M. A. & Battles, D. A. Fluid inclusion and stable isotope analysis of veins from the central Appalachian Valley and Ridge province: Implications for regional syn- orogenic hydrologic structure and fluid migration. *Geol. Soc. Am. Bull.* **111**, 1841–1860 (1999).
47. Seaton, N. C. A., Whitney, D. L., Teyssier, C., Toraman, E. & Heizler, M. T. Recrystallization of high-pressure marble (Sivrihisar, Turkey). *Tectonophysics* **479**, 241–253 (2009).
48. Covey-Crump, S. J. The normal grain growth behaviour of nominally pure calcitic aggregates. *Contrib. Mineral. Petrol.* **129**, 239–254 (1997).
49. Kaczmarek, S. E. & Sibley, D. F. Direct physical evidence of dolomite recrystallization. *Sedimentology* **61**, 1862–1882 (2014).
50. Landing, E., Amati, L. & Franzi, D. A. Epeirogenic transgression near a triple junction: the oldest (latest early-middle Cambrian) marine onlap of cratonic New York and Quebec. *Geol. Mag.* **146**, 552–566 (2009).
51. Kamzolkin, V. A., Ivanov, S. D. & Konilov, A. N. Empirical phengite geobarometer: background, calibration, and application. *Geol. Ore Deposits*. **58**, 613–622 (2016).
52. Roberts, N. M. et al. Laser ablation inductively coupled plasma-mass spectrometry (LA-ICP-MS) U-Pb carbonate geochronology: strategies, progress, and limitations. *Geochronology* **2**, 33–61 (2020).
53. Burisch, M., Markl, G. & Gutzmer, J. Breakup with benefits—hydrothermal mineral systems related to the disintegration of a supercontinent. *Earth Planet. Sci. Lett.* **580**, 117373 (2022).
54. Gebelein, C. D. Biological control of stromatolite microstructure: implications for Precambrian time stratigraphy. *Am. J. Sci.* **274**, 575–598 (1974).
55. Monty, C. L. Spongiostromate vs. porostromate stromatolites and oncolites. In *Phanerozoic Stromatolites* (ed. Monty, C. L.) 1–4 (Springer, 1981).
56. Aragonés Suarez, P. & Leys, S. The sponge pump as a morphological character in the fossil record. *Paleobiology* **48**, 446–461 (2022).
57. Grotzinger, J. P. & Knoll, A. H. Stromatolites in Precambrian carbonates: evolutionary mileposts or environmental dipsticks? *Annu. Rev. Earth Planet. Sci.* **27**, 313–358 (1999).
58. Lee, J. H. & Riding, R. Stromatolite-rimmed thrombolite columns and domes constructed by microstromatolites, calcimicrobes and sponges in late Cambrian biostromes, Texas, USA. *Sedimentology* **70**, 293–334 (2023).
59. Goldring, W. Algal barrier reefs in the lower Ozarkian of New York with a chapter on the importance of coralline algae as reef builders through the ages. *Bull. N. Y. State Mus.* **315**, 5–75 (1938).
60. Neuser, R. D., Bruhn, F., Götze, J., Habermann, D. & Richter, D. K. Kathodoluminseszenz: methodik und Anwendung [cathodoluminescence: method and application]. *Zent bl Geol. Paläontol.* **1**, 287–206 (1996).
61. Bruckschen, P. & Richter, D. K. Zementstratigraphische Grundmuster in marinen Karbonatablagerungen des Phanerozoikums—Ein Abbild der normalen Beckenentwicklung. *Zent bl Geol. Paläontologie Teil I*. **7–8**, 959–972 (1993).
62. Walter, B. F., Immenhauser, A., Geske, A. & Markl, G. Exploration of hydrothermal carbonate magnesium isotope signatures as tracers for continental fluid aquifers, Schwarzwald mining district, SW Germany. *Chem. Geol.* **400**, 87–105 (2015).
63. Goldstein, R. H. & Reynolds, T. J. Systematics of fluid inclusions in diagenetic minerals. *SEPM Soc. Sediment. Geol. Short Course* **31**, 199 (1994).
64. Steele-MacInnis, M., Bodnar, R. J. & Naden, J. Numerical model to determine the composition of H_2O–NaCl–$CaCl_2$ fluid inclusions based on microthermometric and microanalytical data. *Geochim. Cosmochim. Acta* **75**, 21–40 (2011).
65. Bakker, R. J. & Diamond, L. W. Estimation of volume fractions of liquid and vapor phases in fluid inclusions, and definition of inclusion shapes. *Am. Min.* **91**, 635–657 (2006).
66. Beranoaguirre, A., Vasiliev, I. & Gerdes, A. In situ LA-ICPMS U–Pb dating of sulfates: applicability of carbonate reference materials as matrix-matched standards. *Geochronology* **4**, 601–616 (2022).
67. Jochum, K. P. et al. Determination of reference values for NIST SRM 610–617 glasses following ISO guidelines. *Geostand Geoanal. Res.* **35**, 97–429 (2011).
68. Roberts, N. M. et al. A calcite reference material for LA-ICP-MS U-Pb geochronology. *Geochem. Geophys. Geosyst.* **18**, 2807–2814 (2017).
69. Pagel, M. et al. Improving paleohydrological and diagenetic reconstructions in calcite veins and breccia of a sedimentary basin by combining Δ^{47} temperature, $\delta^{18}O$ water and U-Pb age. *Chem. Geol.* **481**, 1–17 (2018).
70. Hill, C. A., Polyak, V. J., Asmerom, Y. & Provencio, P. P. Constraints on a Late Cretaceous uplift, denudation, and incision of the Grand Canyon region, southwestern Colorado Plateau, USA, from U-Pb dating of lacustrine limestone. *Tectonics* **35**, 896–906 (2016).
71. Gerdes, A. & Zeh, A. Zircon formation versus zircon alteration—new insights from combined U-Pb and Lu-Hf in-situ LA-ICP-MS analyses, and consequences for the interpretation of Archean zircon from the Central Zone of the Limpopo Belt. *Chem. Geol.* **261**, 230–243 (2009).
72. Horstwood, M. S. A. et al. Community-derived standards for LA-ICP-MS U-(Th-) Pb geochronology-uncertainty propagation, age interpretation and data reporting. *Geostand Geoanal. Res.* **40**, 311–332 (2016).

Acknowledgements

We thank: E. Rousseau, S. Coté and E. Caraballo Rojas (Université Laval) for thin-section preparation and micro-XRF analyses; M. Born, T. Seemann, and (A) Schulz (Ruhr-University Bochum), and J. Herrero (Universidad Complutense) for additional thin sections and J.M. Cazcarra (National Museum of Natural Sciences, CSIC, Madrid) for their images; R. Hoffmann and M. Alders (Ruhr-University Bochum) for EBSD analysis; S. Wu (Guangxi University) for discussing Triassic (keratosan?) sponges; C. Guilmette (Université Laval), J. Botting (Chinese Academy of Sciences, Nanjing; National Museum Wales), M. McMenamin (Mount Holyoke College), and (B) Murphy (St. Francis Xavier University) for valuable exchange. Journal editor Przemyslaw Gorzelak (Polish Academy of Sciences, Warsaw) guided us through a pretty challenging review process along with constructive comments obtained from V. Paul Wright (PW Carbonate Geoscience, Cardiff) and three anonymous reviewers.

Author contributions
F.N., C.S., S.K. identified the scientific issue and initiated this study. L.A. curated and sent NYSM material. F.N., C.S., S.K. performed basic petrography. M.M. performed advanced petrography, CL-microscopy, EBSD analysis and initiated fluid inclusion analysis and U–Pb dating. B.W. performed fluid inclusion analysis. A.B. performed U–Pb dating. E.L. conceptualized the regional geology. All authors contributed to the editing of the original draft via multiple rounds of internal review.

Competing interests
The authors declare no competing interests.

Additional information
Supplementary Information The online version contains supplementary material available at https://doi.org/10.1038/s41598-024-83359-7.

Correspondence and requests for materials should be addressed to F.N.

Reprints and permissions information is available at www.nature.com/reprints.